JICE - Journal of Infrastructure and Civil Engineering
Vol. 05, No. 3, (November, 2025),
pp. 225-234

Article submitted : 30 10 2025
Review accepted : 28 11 2025
Online Published : 30 11 2025

JICE
JOURNAL OF INFRASTRUCTURE AND CIVIL ENGINEERING
Web: http://jice.sttp-yds.ac.id/index.php/jice/index
ISSN: 2809-5030 (online) 2809-5227 (print)

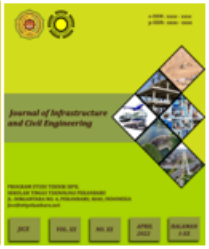

Parametric Analysis of Flexural Strength and Structural Efficiency in Steel I-Beams: The Influence of Depth, Flange Compactness, and Lateral Bracing

Blinka Hernawan Prasetya[1*], Audiyati Ishmata Hani'a[1]

[1] *Department of Civil Engineering, Faculty of Engineering, Universitas Diponegoro*

[*]***Email:*** *blinka@live.undip.ac.id*

Abstract

The flexural design of steel I-beams is governed by a complex interaction between cross-section geometry and stability limits, yet comprehensive comparative data on the performance of compact, non-compact, and slender flange sections across a practical range of depths is often lacking. This study presents a systematic parametric analysis of the nominal flexural strength and structural efficiency of I-sections with depths ranging from 1000 mm to 2500 mm, designed and evaluated in strict accordance with SNI 1729:2020. The investigation considers three distinct flange classifications (compact, non-compact, and slender) under fully, partially, and minimally braced conditions to simulate varying degrees of lateral-torsional buckling (LTB). The results establish a clear performance hierarchy, demonstrating that compact flange sections provide superior strength and material efficiency, achieving up to 18.14 kNm/cm^2. Non-compact sections deliver intermediate capacity, typically 60-64% of compact sections, and are consistently governed by flange local buckling (FLB) for common bracing spacings. Slender sections exhibit severely limited performance, with capacities of only 13-14% of compact sections, rendering them inefficient for primary flexural members. The analysis quantifies the significant economic penalty of inadequate bracing for compact sections, while demonstrating its ineffectiveness for non-compact and slender sections under FLB governance. This research provides a definitive, data-driven framework and practical guidelines for structural engineers to optimize section selection, balancing structural performance with material economy in steel beam design.

Keywords: *flexural strength, flange compactness, lateral-torsional buckling, structural efficiency, parametric analysis*

1. Introduction

Steel I-beams are a common structural element used in buildings, bridges, and industrial structures [1]. Their design is governed by standards that ensure safety and serviceability, such as the Indonesian National Standard known as SNI 1729:2020. This standard provides a framework for flexural design, categorizing beams into different classes based on the slenderness of their flanges and web. These classifications, detailed in Chapters F2 to F5 of the code, range from compact sections that can reach their full plastic moment to slender sections whose strength is limited by elastic buckling. The appropriate design chapter is determined by comparing the width-to-thickness ratios of the flange and web to limiting

https://doi.org/10.35583/jice.v5i3.139

values specified in the code, which accounts for the material's yield strength and modulus of elasticity.

A primary objective in beam design is to achieve sufficient bending capacity, which is functionally related to the section modulus [2], [3]. While a deeper beam generally has a larger section modulus, this does not guarantee a proportional increase in strength. This is because increasing the depth without a corresponding increase in plate thickness leads to greater slenderness, making the section more susceptible to instability.

The instabilities are a central aspect of flexural design and are addressed systematically in SNI 1729:2020. A beam with a slender web may be governed by Web Local Buckling (WLB), where the web buckles before the steel yields. Similarly, a slender compression flange may be susceptible to Flange Local Buckling (FLB) [4]. Furthermore, a beam with insufficient lateral support may fail due to Lateral-Torsional Buckling (LTB) [5], a global instability where the beam twists and deflects sideways.

The code accounts for these limitations through a graduated design approach [6], [7]. A section with a compact web and compact flanges (F2) can develop its full plastic moment. If the web becomes non-compact (F4), its capacity is reduced by a web plastification factor, R_{pc}. If the web is classified as slender (F5), its contribution to bending resistance is significantly reduced by a factor, R_{pg}, and the flexural strength is primarily determined by the flanges. Consequently, the relationship between depth and nominal moment strength is not linear. There exists a point where the benefit of a larger section modulus is counteracted by the reduction in capacity due to slenderness effects.

Other than local buckling, Lateral-Torsional Buckling (LTB) presents a global stability challenge for beams lacking adequate lateral support [8]. This phenomenon involves lateral displacement and twisting of the beam under load, with the buckling behavior categorized into three distinct zones based on the unbraced length (L_b). When L_b is less than or equal to L_p, the beam can develop its full plastic capacity. For unbraced lengths between L_p and L_r, the beam experiences inelastic LTB with reduced capacity. When L_b exceeds L_r, elastic LTB governs with significantly lower moment resistance.

Recent research on steel beam behavior has expanded understanding of both fundamental principles and practical applications. [9] employed genetic algorithms for optimal cross-section geometries that minimize cost while respecting design rules such as bending and shear resistance, M-V interaction, and flange-induced buckling. Niu et al. [10] provided experimental validation of local-global buckling interactions, revealing complex post-buckling behavior that simplified code provisions cannot fully capture. In the Indonesian context, [11] conducted comparative analysis of SNI 1729:2020 with international standards, identifying most efficient design without omitting the regulations. From a sustainability perspective, Bai et al. [12] established quantitative relationships between structural optimization and environmental impact, while [13] developed a multi-objective framework balancing structural performance with carbon emissions.

Recent advances in computational methods have enabled more sophisticated analyses. [14] implemented machine learning techniques to predict beam capacities, achieving accuracy improvements over conventional methods. [15] explored high-strength steel applications, demonstrating different optimal proportions compared to conventional steels. Meanwhile, [16] provided crucial experimental data on hybrid sections, and [17] advanced the direct strength method for slender sections. From a reliability perspective, [18] quantified the safety implications of various optimization approaches.

Despite these contributions, a significant gap persists in systematically mapping the continuous relationship between beam depth and moment capacity across the complete spectrum of SNI 1729:2020 design methodologies. Existing literature provides limited guidance on quantifying the precise depth thresholds where design chapter transitions occur or identifying optimal depth ranges that maximize structural efficiency while considering LTB effects. This gap is particularly relevant for practical design applications where engineers must make informed decisions about beam proportions without comprehensive data on the non-

linear interactions between depth increases, flange compactness, and stability reduction factors.

This study conducts a systematic parametric investigation to address the identified research gaps. The investigation aims to quantify how nominal moment strength varies with beam depth from 1000 to 2500 mm, examining three distinct flange classifications under critical inelastic and elastic lateral-torsional buckling conditions. A key focus is placed on identifying the specific depths at which transitions occur between SNI 1729:2020 design chapters (F2-F5) and on quantifying the associated impact on moment capacity. Based on this analysis, the study will establish optimal depth ranges that maximize structural efficiency for each flange type. The goal is to synthesize these findings into practical design guidance, providing engineers with a clear methodology for selecting beam depths that achieve an effective balance between strength and stability in compliance with SNI 1729:2020.

2. Methodology

This study employed a systematic parametric analysis to investigate the relationship between beam depth and flexural strength across different flange classifications and lateral bracing conditions. The design involved creating a comprehensive matrix of beam configurations by systematically varying key parameters to isolate their effects on flexural behavior according to SNI 1729:2020.

The analysis considered I-sections with constant flange width (b_f = 500 mm) and web thickness (t_w = 12 mm), while systematically varying the beam depth from 1000 mm to 2500 mm in 10 mm increments. Three distinct flange classifications were examined by adjusting flange thickness: compact (t_f = 25 mm), non-compact (t_f = 15 mm), and slender (t_f = 8 mm). The steel material was specified with yield strength F_y = 240 MPa and modulus of elasticity E = 200000 MPa, consistent with commonly used structural steel grades. This parameter matrix resulted in 150 unique beams for each flange configuration for detailed evaluation.

Data was generated through computational analysis based on SNI 1729:2020 specifications. Each beam configuration was systematically classified according to Table B4.1b. Flange compactness was determined by the width-to-thickness ratio λ_f, compared against the limiting values λ_{pf} for compact flanges and λ_{rf} for non-compact flanges. Web slenderness was evaluated using λ_w, with limits of λ_{pw} for compact webs and λ_{rw} for non-compact webs.

The classification outcomes directly determined the applicable design chapter: F2 for sections with compact web and compact flanges; F3 for compact webs with non-compact or slender flanges; F4 for non-compact webs with any flange condition; and F5 for slender webs.

Lateral-torsional buckling effects were incorporated through three unbraced length scenarios: $L_b \leq L_p$ (fully braced), $L_b = 0.5L_r$ (partially braced), and $L_b = L_r$ (minimally braced). The moment gradient factor C_b was conservatively taken as 1.0 for all analyses.

The determination of nominal moment strength followed a systematic procedure where each beam configuration was evaluated according to its governing SNI 1729:2020 design chapter. For each classification, all relevant limit states were comprehensively evaluated, with the final nominal moment strength taken as the minimum value among these limit states.

For F2 sections, the analysis considered yielding ($M_p = F_yZ_x$) and lateral-torsional buckling using Equations F2-2 through F2-4. For F3 sections, lateral-torsional buckling was evaluated alongside compression flange local buckling using Equations F3-1 and F3-2. For F4 sections, the analysis included compression flange yielding (Equation F4-1), lateral-torsional buckling (Equations F4-2 through F4-5), and compression flange local buckling (Equations F4-13 and F4-14), incorporating the web plastification factor R_{pc}. For F5 sections, the bending strength reduction factor R_{pg} was computed (Equation F5-6), and the nominal strength was determined from compression flange yielding (Equation F5-1) and lateral-torsional buckling (Equations F5-2 through F5-5).

To manage the computational complexity, a customized Excel algorithm was developed to automate the section classification process, systematically apply the appropriate equations, and identify the governing nominal moment strength.

The collected data was analyzed through multiple approaches. Flexural strength trends were examined across the depth range for each flange classification and bracing condition. Failure modes were analyzed to explain the observed behavioral patterns and strength characteristics. Structural efficiency was computed as flexural strength per unit cross-sectional area (kNm/cm^2) to evaluate material utilization across different section types. Comparative analysis was performed to establish performance hierarchies and identify critical transition depths where behavioral changes occurred. The results were synthesized to provide practical design recommendations for section selection and optimization according to SNI 1729:2020 requirements.

3. Results and Discussion

This study applied the systematic classification and analysis procedure outlined in previous section to a comprehensive matrix of beam geometries. The results provide a detailed mapping of how flexural strength is governed by the complex interaction of section depth, flange compactness, and lateral bracing. The following discussion interprets the calculated strengths and identifies failure modes through the perspective of the underlying limit state as defined by SNI 1729:2020.

3.1. Flexural strength

Compact flange sections demonstrated the highest flexural capacity across all depth ranges, with generally smooth strength progression linear with the increasing depth. As shown in Figure 1, the fully braced condition (No LTB) showed flexural strength increasing from 3574.8 kNm at 1000 mm to 9869.3 kNm at 2500 mm. This represents the plastic moment capacity (M_p) or compression flange yielding capacity (CFY) achievable when lateral-torsional buckling is prevented.

The inelastic LTB condition maintained approximately 90-95% of the fully braced strength, while the elastic LTB showed more substantial reductions of 35-40%. A notable transition occurred at 1360 mm depth, where the inelastic LTB strength decreased from 4829.6 kNm to 4642.1 kNm despite continued increases in the fully braced beam. This behavior correlates with the web transitioning from compact to non-compact classification (F2 to F4 per SNI 1729:2020), which alters the governing limit state calculations and introduces the web plastification factor (R_{pc}) and the use of elastic section modulus instead of plastic one. The strength recovery observed after this transition indicates that the benefits of increased section modulus eventually overcome the initial penalty imposed by the non-compact web classification. This demonstrates the robust performance of compact flange sections, which maintain superior capacity even as web slenderness increases.

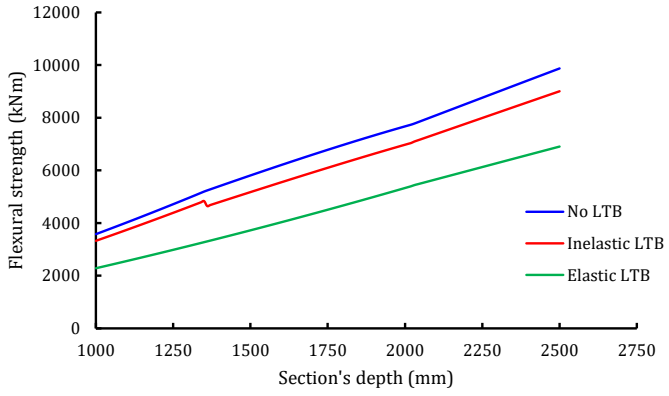

Figure 1. The flexural strength-depth graph of compact flange section

.

Non-compact flange sections exhibited a smooth and consistent increase in strength, characterized by flange local buckling (FLB) governance. As illustrated in Figure 2, the fully braced strength increased from 2131.5 kNm at 1000 mm to 6277.9 kNm at 2500 mm. The identical values for fully braced and the inelastic LTB conditions across all depths confirm that flange local buckling (FLB) consistently governs over inelastic LTB for non-compact sections. Only under the elastic LTB conditions does lateral-torsional buckling become controlling, with additional strength reductions of 22-28%.

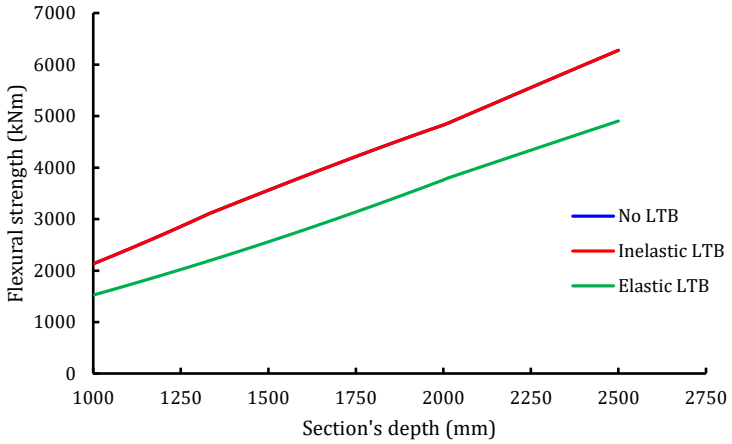

Figure 2. The flexural strength-depth of non-compact flange section

Slender flange sections displayed unambiguous behavior consistent with theoretical expectations. As shown in Figure 3, all three LTB conditions yielded identical strengths at every depth, confirming that flange local buckling (FLB) is the absolute governing limit state. The local instability of slender flanges occurs at stress levels below those required to initiate lateral-torsional buckling, making bracing ineffective for improving flexural capacity. The strength progression was smooth and monotonic, increasing from 475.6 kNm to 1334.3 kNm. This represents only 13-14% of compact section capacity across the depth range, quantifying the severe penalty associated with slender flange elements. The consistent increase in strength reflects that the growing elastic section modulus in the FLB calculation is unaffected by stability considerations.

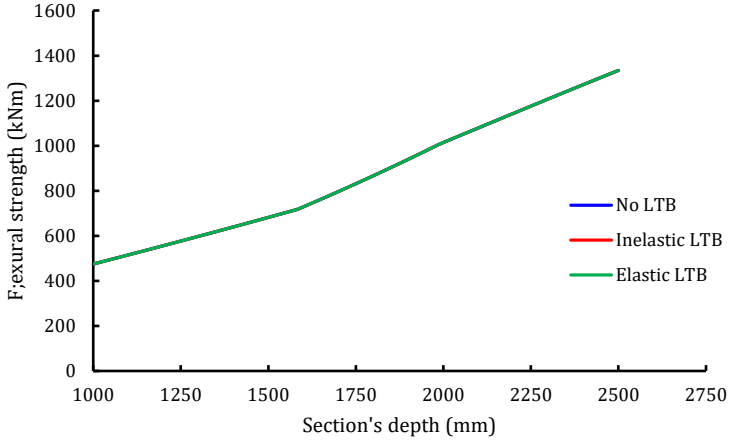

Figure 3. The flexural strength-depth of slender flange section

The relative performance across flange types reveals consistent patterns with important practical implications:

a. Compact sections provide the most reliable and highest performance, with smooth strength progression and predictable LTB effects. Their capacity can be effectively enhanced through strategic bracing, with inelastic LTB maintaining 90-95% of fully braced capacity.
b. Non-compact sections demonstrate intermediate performance, achieving 60-64% of the capacity of equivalent compact sections. Their behavior is governed by flange local buckling for most practical bracing spacings.
c. Slender sections show severely limited capacity that is completely independent of bracing conditions. Their consistently low performance (13-14% of compact capacity) reinforces their unsuitability for primary flexural members in most structural applications.

The data reveals that non-compact sections show slightly improved relative performance at greater depths, reaching 64% of compact capacity at 2500 mm. This suggests that for deep member applications where compact flanges are not feasible, non-compact sections can provide reasonable alternatives. Table 1 shows the flexural strength of each condition.

Table 2. The flexural strength of the beams

Depth (mm)	Flexural strength of compact flange			Flexural strength of non-compact flange			Flexural strength of slender flange		
	No LTB (kNm)	Inelastic LTB (kNm)	Elastic LTB (kNm)	No LTB (kNm)	Inelastic LTB (kNm)	Elastic LTB (kNm)	No LTB (kNm)	Inelastic LTB (kNm)	Elastic LTB (kNm)
1000	3574.800	3320.877	2281.850	2131.498	2131.498	1526.923	475.639	475.639	475.639
1100	4018.800	3737.803	2556.697	2412.199	2412.199	1720.080	516.032	516.032	516.032
1200	4477.200	4165.982	2838.281	2704.643	2704.643	1919.954	556.878	556.878	556.878
1300	4950.000	4605.511	3126.596	3008.829	3008.829	2126.541	598.215	598.215	598.215
1400	5398.903	4793.947	3421.639	3292.164	3292.164	2339.842	640.071	640.071	640.071
1500	5804.572	5171.592	3723.406	3560.200	3560.200	2559.855	682.465	682.465	682.465
1600	6202.132	5545.309	4031.895	3825.184	3825.184	2786.580	729.253	729.253	729.253
1700	6589.443	5913.614	4347.103	4085.714	4085.714	3020.016	797.016	797.016	797.016
1800	6964.369	6275.016	4669.030	4340.390	4340.390	3260.163	867.359	867.359	867.359
1900	7324.768	6628.019	4997.673	4587.812	4587.812	3507.020	940.282	940.282	940.282
2000	7668.501	6971.124	5333.031	4826.579	4826.579	3760.587	1014.648	1014.648	1014.648
2100	8086.756	7376.324	5660.729	5115.975	5115.975	3996.270	1079.281	1079.281	1079.281
2200	8533.350	7783.684	5973.345	5408.038	5408.038	4224.410	1143.767	1143.767	1143.767
2300	8979.767	8190.883	6285.837	5699.478	5699.478	4452.064	1207.901	1207.901	1207.901
2400	9425.307	8597.282	6597.715	5989.636	5989.636	4678.717	1271.475	1271.475	1271.475
2500	9869.265	9002.237	6908.485	6277.852	6277.852	4903.852	1334.282	1334.282	1334.282

3.2. Failure mode

The calculated flexural strengths presented in Figures 1-3 are a direct consequence of the governing limit states for each section, as summarized in Table 2. Analyzing these failure modes provides the critical link between the observed strength values and the underlying physical phenomena presented by SNI 1729:2020.

For compact flange sections, Table 2 confirms a predictable yet depth-dependent progression of failure modes. Under fully braced conditions, the governing limit state transitions from yielding to compression flange yielding (CFY) at a depth of 1360 mm. This shift correlates with the web transitioning from compact to non-compact behavior, making the compression flange more critical in deeper sections. As the unbraced length increases, the failure mode transitions decisively to lateral-torsional buckling (LTB) for both the inelastic LTB' and the elastic LTB conditions. This demonstrates that for well-proportioned sections, global stability becomes the controlling factor when bracing is inadequate.

The behavior of non-compact flange sections is clearly defined by the failure mode data. Table 2 shows that flange local buckling (FLB) governs both the no LTB and the inelastic LTB

conditions across all depths. This explains the identical strength values for these two conditions in Figure 2; the local instability of the flange imposes a strength ceiling that is lower than the inelastic LTB capacity. It is only under the elastic LTB condition, with long unbraced lengths, that the governing limit state shifts to LTB.

The data for slender flange sections is consistent: FLB governs all depths and all unbraced lengths. This finding, consistent across the entire dataset, provides quantitative support for the code's stringent limitations on flange slenderness. It confirms that for slender elements, local instability is the primary and perpetual design concern, rendering investments in lateral bracing completely ineffective for improving flexural capacity.

Table 2. The failure modes of the beams

Depth (mm)	The failure mode of compact flange			The failure mode of non-compact flange			The failure mode of slender flange		
	No LTB	Inelastic LTB	Elastic LTB	No LTB	Inelastic LTB	Elastic LTB	No LTB	Inelastic LTB	Elastic LTB
1000	Yielding	LTB	LTB	FLB	FLB	LTB	FLB	FLB	FLB
1100	Yielding	LTB	LTB	FLB	FLB	LTB	FLB	FLB	FLB
1200	Yielding	LTB	LTB	FLB	FLB	LTB	FLB	FLB	FLB
1300	Yielding	LTB	LTB	FLB	FLB	LTB	FLB	FLB	FLB
1400	CFY	LTB	LTB	FLB	FLB	LTB	FLB	FLB	FLB
1500	CFY	LTB	LTB	FLB	FLB	LTB	FLB	FLB	FLB
1600	CFY	LTB	LTB	FLB	FLB	LTB	FLB	FLB	FLB
1700	CFY	LTB	LTB	FLB	FLB	LTB	FLB	FLB	FLB
1800	CFY	LTB	LTB	FLB	FLB	LTB	FLB	FLB	FLB
1900	CFY	LTB	LTB	FLB	FLB	LTB	FLB	FLB	FLB
2000	CFY	LTB	LTB	FLB	FLB	LTB	FLB	FLB	FLB
2100	CFY	LTB	LTB	FLB	FLB	LTB	FLB	FLB	FLB
2200	CFY	LTB	LTB	FLB	FLB	LTB	FLB	FLB	FLB
2300	CFY	LTB	LTB	FLB	FLB	LTB	FLB	FLB	FLB
2400	CFY	LTB	LTB	FLB	FLB	LTB	FLB	FLB	FLB
2500	CFY	LTB	LTB	FLB	FLB	LTB	FLB	FLB	FLB

3.3. Flexural efficiency

The analysis of nominal flexural strength, while fundamental for assessing structural capacity, does not fully capture the economic considerations essential for practical design. Structural efficiency was measured as flexural strength per unit cross-sectional area. It provides a critical metric for evaluating material utilization and cost-effectiveness.

Figure 4 presents the efficiency trends across all section types and lateral-torsional buckling conditions. Compact flange sections consistently demonstrate superior efficiency, with values progressing from 9.82 kNm/cm^2 at 1000 mm depth to 18.14 kNm/cm^2 at 2500 mm under fully braced conditions. This represents an 85% improvement in material utilization across the depth range investigated. The efficiency advantage of compact sections persists across all bracing conditions, though with predictable reductions as unbraced length increases.

Non-compact flange sections exhibit substantially lower efficiency, resulting at 68-78% of compact section performance. The efficiency progression is smooth, reflecting the consistent increase observed in the dataset. The identical efficiency values for fully braced and the inelastic LTB conditions confirm that flange local buckling (FLB) governs for both, making bracing ineffective for improving material utilization until elastic LTB governs.

Slender flange sections demonstrate profoundly limited efficiency, never exceeding 20% of compact section performance across the entire parameter space. The identical efficiency values across all LTB conditions mirror the strength behavior observed in Figure 3, providing further evidence that no bracing configuration can mitigate the inherent material inefficiency of slender flanges in flexural applications.

Several critical patterns emerge from the efficiency analysis:

a. The rate of efficiency improvement diminishes with increasing depth, particularly beyond 2000 mm, suggesting an economic optimum in the 1500-2000 mm range for most practical applications.

b. The efficiency penalty for inadequate bracing is substantial and quantifiable where compact sections experience 35-42% efficiency reduction when transitioning from fully braced to the elastic LTB conditions.
c. For non-compact sections, the convergence of fully braced and inelastic LTB efficiency curves confirm that bracing investments yield no material utilization benefits for short-to-medium unbraced lengths.
d. The persistent efficiency deficit of slender sections (remaining below 3.53 kNm/cm^2 even at 2500 mm depth) quantifies the severe economic penalty for violating flange compactness limits.

The efficiency trends directly reflect the governing failure mechanisms. The superior efficiency of compact sections stems from their ability to utilize material through ductile yielding. The intermediate efficiency of non-compact sections correlates with their susceptibility to flange local buckling, which limits stress development. The persistently low efficiency of slender sections provides quantitative evidence of the severe material penalty associated with perpetual flange local buckling governance.

These efficiency relationships provide designers with crucial decision-making metrics for balancing structural performance with economic considerations. The data enables quantitative comparison of material utilization across different design strategies, supporting more sustainable and cost-effective structural solutions.

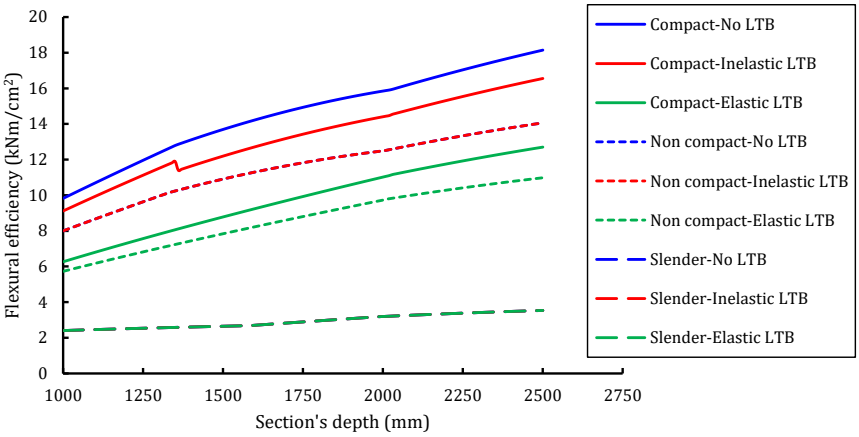

Figure 4. The flexural efficiency of the beams

4. Conclusion

This study has presented a systematic parametric investigation into the flexural behavior of welded steel I-sections, analyzing the interplay between section depth, flange compactness, and lateral bracing. The comprehensive analysis, conducted in accordance with SNI 1729:2020, yields the following definitive conclusions:

a. The classification of flange compactness is the primary determinant of both flexural strength and efficiency. Compact flange sections consistently provide superior performance, achieving strengths of up to 9869 kNm and material efficiencies of up to 18.14 kNm/cm^2. Non-compact sections offer intermediate capacity and efficiency, typically 60-64% and 68-78% of compact sections, respectively. Slender sections are profoundly limited, delivering only 13-14% of the strength and less than 20% of the efficiency of their compact counterparts, rendering them unsuitable for primary flexural members.
b. The governing limit states provide the fundamental explanation for the observed performance. Compact sections fail through desirable ductile mechanisms (yielding or compression flange yielding) when fully braced, transitioning predictably to

lateral-torsional buckling as unbraced length increases. In contrast, non-compact and slender sections are consistently governed by flange local buckling for most practical bracing conditions. This confirms that for non-compact sections, flange strengthening is a more effective strategy than bracing, and for slender sections, no bracing strategy can enhance flexural capacity.

c. The value of lateral bracing is highly dependent on flange compactness. For compact sections, bracing is highly effective, with less braced conditions maintaining 90-95% of fully braced capacity. For non-compact sections, bracing provides no benefit until unbraced lengths become long enough for elastic LTB to govern, as their capacity is otherwise capped by flange local buckling. For slender sections, bracing is entirely irrelevant to flexural strength.
d. While flexural strength and efficiency generally increase in depth, the rate of improvement diminishes, particularly beyond 2000 mm. This suggests an optimum economical depth range of 1500-2000 mm for many applications, where significant capacity is achieved without the diminishing returns associated with very deep, slender web sections.

In summary, this study successfully quantifies the complex interactions that govern the flexural design of steel I-beams. The findings bridge the gap between theoretical code provisions and practical application, providing a clear, data-driven framework for engineers to design safer, more efficient, and more economical steel structures.

References

[1] A. Reka, T. Galinska, D. Ovsii, and M. Hajiyev, "Strengthening of the cross-section of steel i-beams in the tension zone: a review of scientific research," *Academic journal Industrial Machine Building Civil Engineering*, vol. 2, no. 63, pp. 33–38, Dec. **(2024)**, doi: 10.26906/znp.2024.63.3871.

[2] C. T. G. Awodiji and S. Sule, "Probabilistic Assessment of a Doubly Symmetric I-Steel Beam," *Saudi J. Eng. Technol.*, vol. 9, no. 08, pp. 389–396, Aug. **(2024)**, doi: 10.36348/sjet.2024.v09i08.003.

[3] A. Rothwell, "Optimization of Beams," in *Optimization Methods in Structural Design*, vol. 242, in Solid Mechanics and Its Applications, vol. 242. , Cham: Springer International Publishing, **(2017)**, pp. 147–181. doi: 10.1007/978-3-319-55197-5_6.

[4] W. Latif and D. W. White, "Flange Local Buckling Resistance and Local–Global Buckling Interaction in Slender-Flange Welded I-Section Beams," *Eng J*, vol. 59, no. 2, pp. 113–133, June **(2022)**, doi: 10.62913/engj.v59i2.1187.

[5] M. Lebastard, M. Couchaux, A. Bureau, and M. Hjiaj, "Lateral-torsional buckling of uniform and tapered welded I-section beams," *Engineering Structures*, vol. 303, p. 117301, Mar. **(2024)**, doi: 10.1016/j.engstruct.2023.117301.

[6] Y. Zhou, S. Ning, D. Huang, and Y. Li, "Refined plastic hinge method for steel frames with local–global interactive buckling," *Thin-Walled Structures*, vol. 181, p. 110013, Dec. **(2022)**, doi: 10.1016/j.tws.2022.110013.

[7] L. Subramanian and D. W. White, "Flexural Resistance of Longitudinally Stiffened I-Girders. II: LTB and FLB Limit States," *J. Bridge Eng.*, vol. 22, no. 1, p. 04016100, Jan. **(2017)**, doi: 10.1061/(ASCE)BE.1943-5592.0000976.

[8] C. Couto and P. Vila Real, "A proposal based on the effective section factor for the lateral-torsional buckling of beams with slender I-shaped welded sections," *Thin-Walled Structures*, vol. 145, p. 106389, Dec. **(2019)**, doi: 10.1016/j.tws.2019.106389.

[9] J. P. Martins, J. Correia, F. Ljubinković, and L. Simões Da Silva, "Cost optimisation of steel I-girder cross-sections using genetic algorithms," *Structures*, vol. 55, pp. 379–388, Sept. **(2023)**, doi: 10.1016/j.istruc.2023.06.030.

[10] S. Niu, K. J. R. Rasmussen, and F. Fan, "Local–Global Interaction Buckling of Stainless Steel I-Beams. I: Experimental Investigation," *J. Struct. Eng.*, vol. 141, no. 8, p. 04014194, Aug. **(2015)**, doi: 10.1061/(ASCE)ST.1943-541X.0001137.

[11] J. Aloysius, J. A. Sumito, D. Prayogo, and H. Santoso, "Optimization of concentrically braced steel frame structures based on SNI 1726:2019, SNI 1727:2020, SNI 1729:2020, and AISC 341-16," *IOP Conf. Ser.: Earth Environ. Sci.*, vol. 907, no. 1, p. 012010, Nov. **(2021)**, doi: 10.1088/1755-1315/907/1/012010.

[12] J. Bai, K. Yang, Z. Chen, J. Liang, S. Zhang, and Y. Diao, "Geometry and Material Criteria for Low-Carbon Design of I/H-Beams in Sustainable Steel Structures Considering Both Mechanical Properties and Carbon Emissions," *Materials*, vol. 18, no. 21, p. 4930, Oct. **(2025)**, doi: 10.3390/ma18214930.

[13] Z. Zhan, P. Xia, D. Xia, and Y. Hu, "Multi-Objective optimization in the construction of steel-concrete composite columns with carbon emission considerations: Pareto front development and decision-making," *Ain Shams Engineering Journal*, vol. 16, no. 2, p. 103283, Feb. **(2025)**, doi: 10.1016/j.asej.2025.103283.

[14] C. Eshaghi, A. Mazarei, R. Carneiro De Barros, X. Romão, and J. M. Castro, "Machine Learning Approach for Predicting Flexural Behavior Variations of I-Shaped Steel Beams Due to Manufacturing Tolerances," presented at the 9th International Conference on Computational Methods in Structural Dynamics and Earthquake Engineering Methods in Structural Dynamics and Earthquake Engineering, Athens, Greece, **(2023)**, pp. 3433–3444. doi: 10.7712/120123.10650.20816.

[15] A. Su *et al.*, "Unified machine-learning-based design method for normal and high strength steel I-section beam–columns," *Thin-Walled Structures*, vol. 199, p. 111835, June **(2024)**, doi: 10.1016/j.tws.2024.111835.

[16] K. Saini, R. Lalthazuala, and T. G. Singh, "Flexural behaviour of hybrid high-strength steel I-beams," *Steel and Composite Structures*, vol. 55, no. 4, pp. 319–332, May **(2025)**, doi: 10.12989/SCS.2025.55.4.319.

[17] R. S. Glauz, "Enhancements to the Direct Strength Method of cold-formed steel member design," *Thin-Walled Structures*, vol. 183, p. 110421, Feb. **(2023)**, doi: 10.1016/j.tws.2022.110421.

[18] A. Tarawneh, O. Alajarmeh, R. Alawadi, H. Amirah, and R. Alramadeen, "Database evaluation and reliability calibration for flexural strength of hybrid FRP/steel-RC Beams," *Composite Structures*, vol. 329, p. 117758, Feb. **(2024)**, doi: 10.1016/j.compstruct.2023.117758.